Interatomic Coulombic decay of fixed-in-space neon dimers

S. K. Semenov,[1,2] K. Kreidi,[2] T. Jahnke,[2] Th. Weber,[3] T. Havermeier,[2] R. E. Grisenti,[2] X. Liu,[4] Y. Morisita,[4] L. Ph. H. Schmidt,[2] M. S. Schöffler,[2] M. Odenweller,[2] N. Neumann,[2] L. Foucar,[2] J. Titze,[2] B. Ulrich,[2] F. Sturm,[2,3] H. K. Kim,[2] K. Ueda,[4] A. Czasch,[2] O. Jagutzki,[2] N. A. Cherepkov,[1,2] and R. Dörner[2]

[1]*State University of Aerospace Instrumentation, 190000, St. Petersburg, Russia*

[2]*Institut für Kernphysik, University Frankfurt, Max-von-Laue-Strasse 1, D-60438 Frankfurt, Germany*

[3]*Lawrence Berkeley National Laboratory, Berkeley, California 94720, USA*

[4]*Institute of Multidisciplinary Research for Advanced Materials, Tohoku University, Sendai 980-8577, Japan*

(Received 4 November 2011; published 24 April 2012)

The detailed theoretical and experimental analysis of the angular distributions of electrons from interatomic Coulombic decay (ICD) of the Ne dimer in the molecular frame is performed. In the initial state the doubly charged dimer ion has one $2s$ vacancy and one $2p$ vacancy on one atom. After the ICD process the neutral neon atom is ionized and the triply charged molecular ion dissociates into singly and doubly charged atomic ions, $Ne^{2+}(2p^{-2}) + Ne^{+}(2p^{-1})$. From the coincident measurement of kinetic energy release (KER) of the ions and the ICD electron the decay channel can be identified unambiguously. The most detailed experimental data have been obtained for the singlet dicationic state $Ne^{2+}(2p^{-2})[^1D]$. Different KER energies correspond to different internuclear distances at which the ICD process takes place. In experiment the data have been presented for three regions of KER energies, and the corresponding calculations have been performed for three fixed internuclear distances. In calculations we imply that all the electrons in Ne_2 to a good approximation are localized. However, we need to retain the molecular character of the dimer wave functions which opens the possibility for the ICD process. To do it, we calculate at first the Hartree-Fock ground state wave functions of the neutral Ne_2 dimer using the standard procedure for homonuclear diatomic molecules corresponding to the $D_{\infty h}$ symmetry group. For the doubly charged ion $Ne_2{}^{2+}$ with two vacancies on one atom the symmetry is lowered to $C_{\infty v}$, and we are looking now for the set of one-electron Hartree-Fock wave functions which are localized either on the left or on the right atom as a linear combination of symmetry-adopted wave functions. The theory correctly reproduces the experimental data and predicts the sharp variation of the angular distributions as a function of internuclear distance.

DOI: 10.1103/PhysRevA.85.043421 PACS number(s): 33.80.Eh

I. INTRODUCTION

Ionization of atoms and molecules by photons with energy exceeding the second ionization threshold can produce an electronically excited state which decays by releasing the excess energy by emission of either a photon or an electron. The radiative lifetime is usually on the order of nanoseconds. If the Auger decay is energetically allowed, the corresponding Auger lifetime is much shorter and varies from several femtoseconds to several tens of femtoseconds. For many decades the Auger decay processes of atoms and molecules have been used as a tool to study their structure [1]. When an inner-valence vacancy is produced in an isolated atom, it usually does not possess sufficient energy for the Auger decay and decays only radiatively, so that the corresponding vacancies are rather long-lived. Recently, Cederbaum *et al*. [2,3] proposed a new mechanism of electronic decay of loosely bound systems like rare gas dimers and clusters bound by the van der Waals forces. In these cases the individual atoms are only weakly disturbed by their neighbors, but that is sufficient to open the electronic decay channel for inner-valence vacancy and in that way to shorten the lifetime of the inner-valence-excited states dramatically. In the particular case of isolated Ne atom the $2s$ vacancy does not possess sufficient energy for the Auger decay into the final state with two $2p$ vacancies, while in the Ne_2 dimer this energy is sufficient for producing two singly charged Ne ions, each having one vacancy in the $2p$ shell, $Ne_2^{+}(2s^{-1}) \rightarrow Ne^{+}(2p^{-1}) + Ne^{+}(2p^{-1})$. Such a process was called interatomic (or intermolecular) Coulombic decay (ICD) [3].

Stimulated by this theoretical prediction of Cederbaum *et al*. [2,3], several experimental studies were soon published. At first the ICD processes were detected in Ne and Ar clusters [4–6] by observing the additional lines in the photoelectron spectra after creation of the inner-valence vacancy. In a much more detailed study of the $2s$-ionized Ne dimers by Jahnke *et al*. [7] using the electron-ion-ion coincidence technique the ICD electron energy distribution was measured simultaneously with the kinetic energy release (KER) distribution of two Ne^{+} ions. A good agreement with the theoretical prediction for the ICD electron energy distribution by Cederbaum *et al*. was demonstrated. The ICD process of resonantly excited Ne_2 dimers was studied in [8]. The most detailed experimental study of the ICD process in the $2s$-ionized Ne dimers was presented in [9], where the angular distributions of photoelectrons and of the ICD electrons in the molecule-fixed (or more precisely dimer-fixed) frame have been measured. These measurements are possible because the rotational period of Ne dimers is much longer than the ICD decay time. Since the final state (two singly charged Ne ions) in these studies is symmetric relative to reflection in the plane perpendicular to the dimer axis, the angular distributions possess the reflection symmetry, too, and there is no way to determine in which atom the original vacancy has been produced. On the other hand, in recent years the problem of the core hole localization in different molecules has attracted much attention (see [10–14] and references therein). In N_2 the most sophisticated experimental data for the photoelectron–Auger-electron angular correlations

in the molecule-fixed frame have been successfully interpreted from the standpoint of coherently populated delocalized core hole states [14]. Contrary to that, in Ne dimers, due to the substantially larger internuclear distance, the core hole to a good approximation is expected to remain localized for a long time. To prove it experimentally one needs to study a process in which the atom with the original core hole produced by the photoabsorption can be distinguished from the neighboring neutral atom in the dimer. The way to do it was proposed by Santra and Cederbaum in [15].

Suppose that the original vacancy in the dimer is created not in the inner valence but in the core shell. The subsequent intra-atomic Auger decay can produce, among others, the doubly charged ion with one vacancy in the inner-valence shell and the other one in the valence shell. In the particular case of the Ne dimer it means that the photoionization creates the $1s$ hole which, after the Auger decay, produces the doubly charged ion with one hole in the $2s$ shell and the other one in the $2p$ shell. This state does not possess sufficient energy for the next Auger decay within the monomer, but this energy is sufficient for ionizing the neighbor neutral Ne atom. As was shown in [15], even though the dimer is bound by rather weak van der Waals forces, they are sufficient for opening the ICD decay channel producing the singly and the doubly charged ions, $Ne^{2+}(2p^{-2}) + Ne^{+}(2p^{-1})$. The measurements made for Ar dimers in [16] using the ICD electron-ion-ion coincidence technique unambiguously demonstrated the existence of this decay channel. More detailed studies have been made for Ne dimers in [17,18] using the electron-ion-ion coincidence technique. The molecular frame photoelectron angular distributions measured in these papers are in a qualitative agreement with the corresponding theoretical curves obtained in the Hartree-Fock approximation [17] and the time-dependent density functional theory [18]. Kreidi *et al.* [17] have measured also the molecular frame ICD electron angular distributions. Up to now there were no theoretical calculations for comparison with this experiment. It is the goal of this paper to present the theoretical results for the molecule frame ICD electron angular distributions resulting from the core photoionization of Ne dimers.

The ICD process is analogous to the Auger decay and is caused by the Coulomb interaction between electrons. The method to calculate the molecule frame Auger electron angular distributions produced by the decay of the K-shell vacancy in N_2 molecule has been developed in [12,19–21]. In that case the core holes are delocalized, and the comparison between theory and experiment clearly demonstrated the existence of the separate Auger decay channels of the gerade and ungerade core hole states. In the case of Ne_2 dimer the two neon atoms are well separated, and to a good approximation one can consider the deep valence hole in each Ne atom as being localized. Therefore, the approximation developed in [19,21] was modified in order to take into account this localization. On the other hand, the very existence of the ICD process tells us that the field of the neighboring atom must be taken into account. The method proposed in this paper combines both peculiarities, the localization of the deep valence hole and the existence of the molecular field.

Atomic units are used in the paper unless otherwise stated in the text.

II. CLASSIFICATION OF THE ICD PROCESSES

The most detailed theoretical description of the ICD processes in Ne dimers was given by Stoychev *et al.* in [22]. We are using their results for the energy levels of all intermediate and final states as the starting point for our consideration. Our study concentrates on the molecule frame ICD electron angular distributions which have not been calculated up to now. Therefore, the initial state for our consideration is the doubly charged Ne_2^{2+} ion with one $2s$ vacancy and one $2p$ vacancy on the same atom which we will denote as the atom No. 1 (or the left atom). The full description of this state is $Ne^{2+}(2s^{-1}2p^{-1})[^1P]$-Ne. The similar triplet state $Ne^{2+}(2s^{-1}2p^{-1})[^3P]$ lies below the threshold for the triple ionization of the Ne dimer and therefore is not discussed in this paper.

We present in the following the ICD processes by Feynman diagrams frequently used in many-body perturbation theory as described, for example, in [23,24]. The processes starting from the photoionization of the $1s$ shell, the subsequent Auger decay (denoted by the letter A below), and finally the ICD are shown in Fig. 1(a). Here the dashed line is the photon ($h\nu$), the wavy line is the Coulomb interaction, and the solid lines present either particles (with arrows from the left to the right) or holes (with arrows from the right to the left). Time is increasing from the left to the right. The notations $n(1)$, $n'(1)$, $n''(2)$ are introduced in order to distinguish between different hole states and hole positions in the molecule. The vertical up and down arrows indicate the projection of spin of the hole states. This diagram corresponds to the sequence of the processes according to the equation

$$\begin{aligned}(\mathrm{Ne}-\mathrm{Ne})+h\nu &\rightarrow \{\mathrm{Ne}^{+}(1s^{-1})[^2S]-\mathrm{Ne}\}+e^{-}_{ph}\\ &\rightarrow \{\mathrm{Ne}^{2+}(2s^{-1}2p^{-1})[^1P]-\mathrm{Ne}\}+e^{-}_{ph}+e^{-}_{A}\\ &\rightarrow \{\mathrm{Ne}^{2+}(2p^{-2})[^1D]-\mathrm{Ne}^{+}(2p^{-1})[^2P]\}\\ &\quad +e^{-}_{ph}+e^{-}_{A}+e^{-}_{\mathrm{ICD}}. \qquad (1)\end{aligned}$$

In Fig. 1(b) we show the corresponding exchange diagram (in the first Auger decay) which is described by the same equation (1) and which leads to the same final state. In our study of the angular distribution of the ICD electrons we consider only the process described by the last line of Eq. (1). Therefore, we draw in Fig. 1(c) separately the part of the diagrams shown in Figs. 1(a) and 1(b) responsible for the ICD process which is characterized by one Coulomb matrix element. Actually there are two kinds of the ICD process, the direct and the exchange. In the direct process the $2s(1)$ vacancy is filled by the $2p(1)$ electron from the same atom as is shown in Figs. 1(a), 1(b), and 1(c), while in the exchange process the $2s(1)$ vacancy is filled by the $2p(2)$ electron from the neighboring atom, as is shown by the diagram in Fig. 1(d). We denote below the direct and the exchange ICD processes by dICD and eICD, respectively. The doubly charged ion $Ne^{2+}(2p^{-2})$ can be in the states with three different terms: ^1S, ^1D, and ^3P. From the potential energy curves obtained in [22] and presented in Fig. 2 it follows that the highest of them, ^1S, is accessible to the ICD only at rather large internuclear distances, above 7 a.u., which is substantially larger than the equilibrium distance about 5.9 a.u (about 3.1 Å). As was mentioned earlier, the Auger and ICD processes are rather fast, and the internuclear

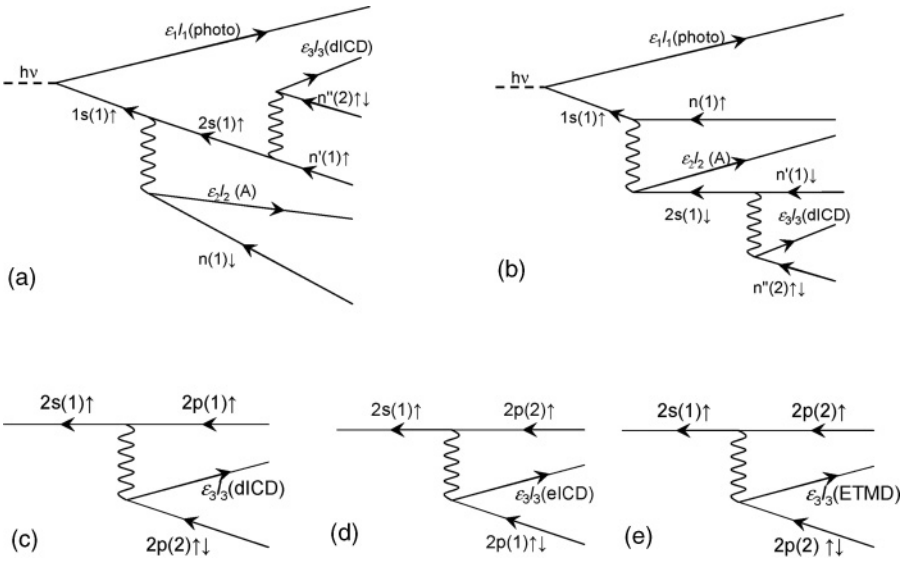

FIG. 1. Feynman diagrams showing the processes (1) studied in this paper (see the text for further details). The vertical up and down arrows indicate the projection of spin of the hole states. (a) The diagram showing all three processes: the photoionization, the Auger decay, and the direct ICD process. (b) The same as in (a) but corresponding to the exchange process in the Auger decay. (c)–(e) The parts of the diagram (a) representing the direct ICD process (c), the exchange ICD (d), and the ETMD process (e).

distance during these processes remains nearly unchanged. Therefore, the contribution of different internuclear distances is characterized by the vibrational wave function of the initial state of Ne_2. Although the zero vibrational wave function of Ne_2 is quite broad, only a small fraction of its tail will spread at the distance above 7 a.u. Therefore, the probability of the corresponding transition is expected to be negligible [22]. As to the ^3P term, the transition to it from the singlet initial state $Ne^{2+}(2s^{-1}2p^{-1})[^1P]$ within one atom is forbidden without a spin-flip of the $2p(1)$ electron. Inclusion of spin-orbit coupling makes this transition possible, although its probability, according to the estimation made in [22], is very small. Therefore, we imply that the decay process given by Eq. (1) is the only process contributing to the direct ICD channel.

In the exchange ICD process shown in Fig. 1(d) the $2s(1)$ vacancy is filled by the electron from the neighboring atom, $2p(2)$, while the excess energy is transferred to the $2p(1)$ electron which can have either up or down spin projection. As a result, both terms of the $Ne^{2+}(2p^{-2})$ state, ^1D and ^3P, are contributing. In the case of the ^1D term the final states for the direct and exchange ICD processes are identical, and Eq. (1) describes also the exchange ICD. The corresponding direct and exchange channels interfere. For the triplet final state $Ne^{2+}(2p^{-2})[^3P]$ the equation describing this eICD process is

$$\{Ne^{2+}(2s^{-1}2p^{-1})[^1P] - Ne\} \rightarrow \{Ne^{2+}(2p^{-2})[^3P] - Ne^{+}(2p^{-1})[^2P]\} + e^{-}_{eICD}. \quad (2)$$

Since the energy of the $Ne^{2+}(2p^{-2})[^3P]$ state is about 4 eV lower than that of the $Ne^{2+}(2p^{-2})[^1D]$ state, the excess energy in this process is larger than in the process (1). Because of that there is no interference between the decay channels into the $Ne^{2+}(2p^{-2})[^3P]$ and $Ne^{2+}(2p^{-2})[^1D]$ states.

Finally, Fig. 1(e) shows another possible decay process when the vacancy in the $2s(1)$ shell is filled by the $2p(2)$ electron, and the excess energy is transferred to another $2p(2)$ electron. This process was termed in [22] electron-transfer-mediated decay (ETMD). Here again the $Ne^{2+}(2p^{-2})$ ion can be either in ^1D or in ^3P state. The equations describing the ETMD are

$$\{Ne^{2+}(2s^{-1}2p^{-1})[^1P] - Ne\} \rightarrow \{Ne^{+}(2p^{-1})[^2P] - Ne^{++}(2p^{-2})[^3P]\} + e^{-}_{ETMD},$$
$$\{Ne^{2+}(2s^{-1}2p^{-1})[^1P] - Ne\} \rightarrow \{Ne^{+}(2p^{-1})[^2P] - Ne^{++}(2p^{-2})[^1D]\} + e^{-}_{ETMD}. \quad (3)$$

There is no interference between the ETMD and ICD since the doubly charged ions in these processes are on the opposite sites.

III. THEORY

The starting point of our theoretical consideration is the dicationic singlet state of the Ne_2^{2+} dimer produced by photoionization of the $1s(1)$ shell of the left Ne atom and by the subsequent Auger decay on the same atom. As a result,

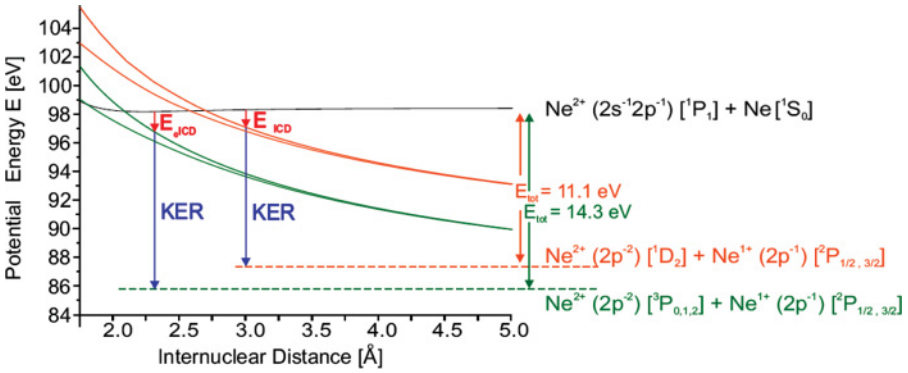

FIG. 2. (Color online) Potential energy curves describing the two-site tricationc states populated by ICD (upper curves) and eICD (lower curves) decay channels. The KER energies for these states are also shown in the figure.

in the Ne_2^{2+} ion the left atom is doubly ionized and the right atom is neutral. In our numerical calculations of the ICD and ETMD processes we imply that all the electrons in the Ne dimer to a good approximation are localized. On the other hand, we would like to retain the molecular character of the dimer wave functions (that is the axial symmetry of the problem), even though the van der Waals force connecting the two Ne atoms is weak. In this way we are taking into account, in particular, the scattering of the ICD and ETMD electrons on the neighboring atom of the dimer, which is not negligible at all. To realize it in practice, we calculate at first the Hartree-Fock (HF) ground-state wave functions of the neutral Ne_2 dimer using the standard procedure for homonuclear diatomic molecules belonging to the $D_{\infty h}$ symmetry group. In that way we obtain the set of single-particle wave functions for the $1\sigma_g, 1\sigma_u, 2\sigma_g, 2\sigma_u, 3\sigma_g, 3\sigma_u, 1\pi_g$, and $1\pi_u$ molecular states. For the doubly charged ion Ne_2^{2+} with two vacancies on one atom the symmetry is lowered to the $C_{\infty v}$. We are looking now for the set of one-electron wave functions which are localized either on the left atom or on the right atom (spin wave functions are omitted here) according to the definitions

$$\begin{aligned}
\varphi_{1s}^{(1)} &= \varphi_{1\sigma_g} + \varphi_{1\sigma_u}, \quad \varphi_{1s}^{(2)} = \varphi_{1\sigma_g} - \varphi_{1\sigma_u}, \\
\varphi_{2s}^{(1)} &= \varphi_{2\sigma_g} + \varphi_{2\sigma_u}, \quad \varphi_{2s}^{(2)} = \varphi_{2\sigma_g} - \varphi_{2\sigma_u}, \\
\varphi_{2p\sigma}^{(1)} &= \varphi_{3\sigma_g} + \varphi_{3\sigma_u}, \quad \varphi_{2p\sigma}^{(2)} = \varphi_{3\sigma_g} - \varphi_{3\sigma_u}, \\
\varphi_{2p\pi}^{(1)} &= \varphi_{1\pi_g} + \varphi_{1\pi_u}, \quad \varphi_{2p\pi}^{(2)} = \varphi_{1\pi_g} - \varphi_{1\pi_u}.
\end{aligned} \tag{4}$$

Omitting below in the Slater's determinants all doubly occupied spin orbitals one can write the initial singlet state wave function of the ion as

$$\begin{aligned}
\Psi_i^{N-2} &= \frac{1}{\sqrt{2}}\{\|\varphi_{2s\uparrow}^{(1)}, \varphi_{n\downarrow}^{(1)}, \ldots\| - \|\varphi_{2s\downarrow}^{(1)}, \varphi_{n\uparrow}^{(1)}, \ldots\|\} \\
&\equiv \frac{1}{\sqrt{2}}\{\Phi_{\uparrow\downarrow} - \Phi_{\downarrow\uparrow}\}.
\end{aligned} \tag{5}$$

Here the $\uparrow, \downarrow$ signs correspond to the $+1/2$ or $-1/2$ projections of spin, n is one of the states

$$n = 2p\sigma,\ 2p\pi_+,\ 2p\pi_-, \tag{6}$$

and π_+, π_- mean the states with the projection of orbital angular momentum equal to $+1$ or -1, respectively. Using these wave functions as an initial approximation, we solve in the usual way the self-consistent HF equations for the Ne_2^{2+} state with two holes localized on the left atom as if it were a *heteronuclear* diatomic molecule. It means that both even and odd spherical harmonics are contributing to these wave functions. The solutions of these equations are used as the basis set for the further calculations. In the following all the wave functions of the dimer will be characterized according to Eq. (6) and Eqs. (1)– (3), where the projection of the orbital angular momentum is not mentioned and must be considered only as a simplified notation. As an example, Fig. 3 shows the wave functions of the $2s$ and $2p\sigma$ bound states calculated by this method. They are strongly localized at the specified centers, though there is some probability for the electrons to be observed near the neighboring atom. Therefore, all the results obtained with these localized wave functions will be different from the pure atomic calculations. In particular, the angular distributions of photoelectrons obtained in this way

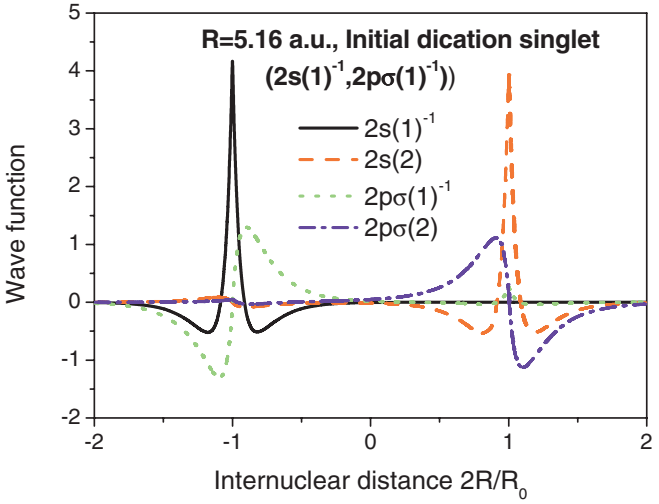

FIG. 3. (Color online) The wave functions of the localized hole states $2s(1)^{-1}$ and $2p\sigma(1)^{-1}$ and localized particle states $2s(2)$ and $2p\sigma(2)$.

and published in Fig. 3 of Ref. [17] show a strong left-right asymmetry which does not appear in the pure atomic picture.

The wave functions of the ICD or ETMD electrons are calculated in two different approximations. In one case the field of the frozen core of the triply charged dimer ion is constructed from the wave functions of the doubly charged state, with orthogonalization to the basis set of the initial orbitals. These wave functions correspond to a kind of the usual "frozen core" HF approximation. The other possibility is to calculate self-consistently the HF wave function of the triply charged ion in the final state, and after that the wave function of the ICD or ETMD electron is calculated in the frozen field of this ion. That is a kind of "relaxed core" HF approximation. Now the final-state wave function is not orthogonal to the initial-state wave function Ψ_i^{N-2}, and the overlap integrals must be included in the calculations of the transition matrix elements. We calculate the overlap matrix between the HF orbitals of the initial and final states $\mathbf{S}_{jk} = \langle\varphi_j^{(f)}|\varphi_k^{(i)}\rangle$ and obtain the Auger amplitudes following the procedure proposed in [25]. We calculated the ICD angular distributions using both the "frozen core" and relaxed core approximations.

Using the wave functions defined above, the ICD amplitudes are calculated by the equation (see [15])

$$\begin{aligned}
A_{f,i}^{\mathrm{ICD}} &= \langle\Phi_f||r - r'|^{-1}|\Phi_i\rangle \\
&= \sqrt{2}\langle\varphi_{\mathbf{k}}^-(r), \varphi_{2s}^{(1)}(r')||r - r'|^{-1}|\varphi_{n''}^{(2)}(r), \varphi_{n'}^{(1)}(r')\rangle \\
&\quad - \frac{1}{\sqrt{2}}\langle\varphi_{\mathbf{k}}^-(r), \varphi_{2s}^{(1)}(r')||r - r'|^{-1}|\varphi_{n'}^{(1)}(r), \varphi_{n''}^{(2)}(r')\rangle,
\end{aligned} \tag{7}$$

which is a difference of the direct and the exchange terms. Here $n', n'' = 2p\sigma, 2p\pi_+, 2p\pi_-$, and $\varphi_{\mathbf{k}}^-(r)$ is the ICD (or ETMD) electron wave function with the momentum $\mathbf{k}$. In the asymptotic region of large r it contains a superposition of a plane wave propagating in the direction of the electron momentum $\mathbf{k}$ and a converging spherical wave. For the triplet $Ne^{2+}(2p^{-2})[^3P]$ final state the direct ICD process is symmetry

forbidden, and only the second (the exchange) term in this equation remains. The amplitude of the ETMD process is calculated in a similar way,

$$A_{f,i}^{\mathrm{ETMD}} = \langle \Phi_f || r - r' |^{-1} | \Phi_i \rangle \propto \left[\left\langle \varphi_{\mathbf{k}}^{-}(r), \varphi_{2s}^{(1)}(r') \middle| |r - r'|^{-1} \middle| \varphi_{n''}^{(2)}(r), \varphi_{n'}^{(2)}(r') \right\rangle \pm \left\langle \varphi_{\mathbf{k}}^{-}(r), \varphi_{2s}^{(1)}(r') \middle| |r - r'|^{-1} \middle| \varphi_{n'}^{(2)}(r), \varphi_{n''}^{(2)}(r') \right\rangle \right], \quad (8)$$

where the plus sign corresponds to the singlet state $Ne^{2+}(2p^{-2})[^1D]$, the minus sign to the triplet state $Ne^{2+}(2p^{-2})[^3P]$, and $n' \neq n''$. If $n' = n''$, only the first term remains in this equation.

The angular distribution of the ICD (or ETMD) electrons is defined by the equation

$$I_{f,i}^{\mathrm{ICD}} = \left| A_{f,i}^{\mathrm{ICD}} \right|^2 . \quad (9)$$

IV. EXPERIMENT

The experiment has been performed at the beamline UE56/1 SGM at BESSY (Berlin) using the COLTRIMS technique [26–29]. The experimental setup is identical to one described in [17,27]. The beam of linearly polarized photons was crossing with a supersonic Ne gas beam. At a driving pressure of about 7.5 bar, 160 K temperature the neon gas was expanded through a 30-μm-diameter nozzle. This resulted in a fraction of dimers to monomers of about 1%. From the overlap region of gas and photon beam (about $0.5 \times 0.5 \times 3$ mm^3) the charged particles were guided by parallel magnetic ($B = 6$ G) and electric ($E = 20$ V/cm) fields toward two position-sensitive delay-line detectors with multihit capability [30]. The spectrometer has a solid angle of detection of 4π for electrons of energy up to 12 eV. For the data presented here we analyzed data where we detected both ions and one electron in a triple coincidence. This triple coincidence was sufficient to suppress the background resulting for ionization of the monomers in the gas jet.

The ion charge state and momentum vectors were obtained from the measurements of the time of flight and positions of impact. Since the final state of the Ne^{1+} Ne^{2+} potential energy curves are steeply repulsive (close to $2/R$), the fragmentation is fast compared to any rotation and the fragmentation direction of the back-to-back emitted ions closely resembles the orientation of the internuclear axis at the instant of emission of the ICD electron. In that way we obtain the angular distributions of the ICD electron in the body-fixed frame of the dimer.

From the coincident measurement of kinetic energy release of the ions and the ICD or ETMD electron the decay channel of Eqs. (1)– (3) can be identified unambiguously. For a complete overview of all channels, we refer to Ref. [27]. For the current purpose the relevant figure from [27] is adapted here in Fig. 4. The diagonal A in Fig. 4 is formed by the contributions of three processes, ICD direct, ICD exchange, and ETMD for the case of the $Ne^{2+}(2p^{-2})[^1D]$ doubly charged ion state [Eqs. (1) and (3b)]. The diagonal B is the sum of the ICD exchange and the ETMD contributions corresponding to the $Ne^{2+}(2p^{-2})[^3P]$ ion state [Eqs. (2) and (3a)].

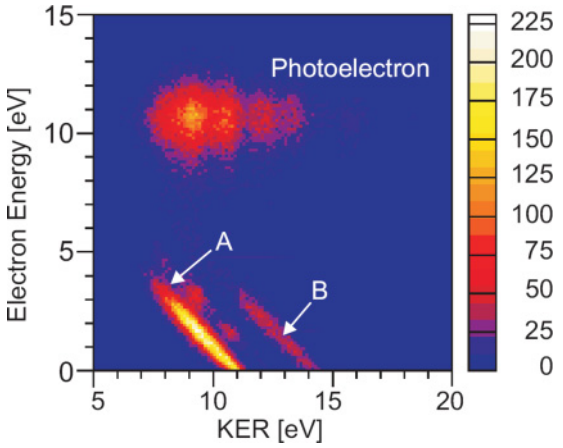

FIG. 4. (Color online) The kinetic energy of the ionic fragments in dependence of the electron energy. The photon energy is 881.2 eV, resulting in an energy of the 1s photoelectron of 11 eV. The two diagonal lines A and B correspond to the creation of the singlet $Ne^{2+}(2p^{-2})[^1D]$ and triplet $Ne^{2+}(2p^{-2})[^3P]$ final states of the doubly charged neon ion, respectively (adapted from [27]).

V. DISCUSSION OF THE RESULTS

Let us start the discussion from the angular distributions of the ICD electrons. In experiment both the ICD electron energy and the KER of two departing ions have been measured simultaneously. Different KER energies correspond to different internuclear distances at which the ICD process takes place. Evidently, the angular distributions of the ICD electrons depend on the internuclear distance. The experimental data obtained in three regions of KER energies are shown in Fig. 5. The dependence on the KER energy is apparent. With the increasing of KER energy the electron intensity in the direction of the Ne^+ ion is increasing, while, in general, the shape of the angular distribution does not change dramatically. The corresponding theoretical angular distributions obtained at three fixed internuclear distances are also shown there. Since the experimental data do not give the absolute values of the yield, we normalized our theoretical data to the maximum of the experimental angular distribution. The calculations have been performed according to Eq. (7) as a difference of the direct and the exchange terms for all possible combinations of the states n' and n''. Both the frozen core and the relaxed core HF approximations described above have been used. In both cases there is a reasonable agreement with the experimental data. The main peculiarity, the increase of the intensity in the direction of the Ne^+ ion with increasing of KER energy (that is with decreasing of the internuclear distance R) is reproduced by the theory. In all cases the relaxed core method underestimates the relative magnitude of the Ne^+ maximum, while the frozen core method overestimates it. The difference between the results of two methods gives the estimation of the contribution of many-electron correlations partially taken into account in our FCHF and RCHF calculations. As to the absolute values of the ICD intensity as a function of the internuclear distance R, the intensity at $R = 4.8$ is about factor of 5 larger than the intensity at $R = 6.8$. The shapes of the angular distributions depend on both the ICD electron energy and the internuclear

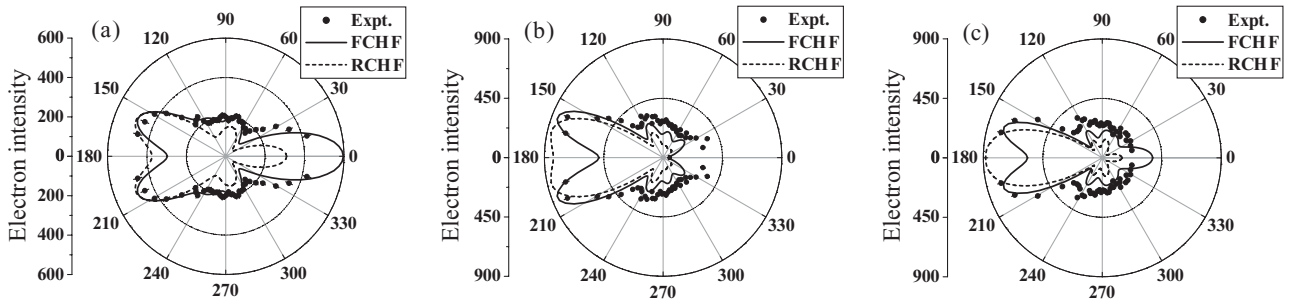

FIG. 5. The experimental (points) and theoretical (curves) angular distributions of the ICD electrons corresponding to the singlet final state $Ne^{2+}(2p^{-2})[^1D]$ [Eqs. (1) and (3b) (line A in Fig. 4)]. Experimental data: (a) KER = 10–11.1 eV, (b) KER = 9–10 eV, (c) KER = 7–9 eV. Theoretical data are obtained in the frozen core (dashed lines) and relaxed core (solid lines) HF approximations. The calculations have been performed at $R = 4.8$ a.u., $k = 0.05$ (a); $R = 5.67$ a.u., $k = 0.343$ (b); and $R = 6.8$ a.u., $k = 0.477$ (c). The molecular axis is horizontal with the doubly ionized neon atom in the initial state on the left side.

distance. We made several test calculations for a fixed R and different ICD electron energies and found that the shape of the angular distribution is mainly defined by the internuclear distance.

In Fig. 6 we show the partial contributions of several ICD channels corresponding to different $n',n'' = 2p\sigma$, $2p\pi_{\pm}$ states which give the main contribution to the total intensity. The corresponding Feynman diagrams are also shown there. In Fig. 6(a) we show the contribution of the ICD transition producing the σ ICD electron. The main intensity is directed along the molecular axis as it should be for the s waves. From the left-right asymmetry of the angular distribution one can conclude that both even and odd partial waves are giving equally important contributions. The presence of the additional lobe at the angle of about 115° (and 245°) tells us that relatively high partial waves are contributing. Calculations for all other transitions creating the σ ICD electron show that the shapes of these angular distributions are qualitatively similar, and they differ mainly by magnitudes. Therefore, we show here only one transition of this kind. In Fig. 6(b) another process is shown from which the π ICD electron is emitted. Now the intensity along the molecular axis is zero, and again there is a strong left-right asymmetry. The calculations for other transitions with π ICD electrons show that they also have similar shapes and differ mainly by magnitudes. Finally, in Fig. 6(c) we show the angular distribution produced by the δ ICD electron. The intensity of this term is relatively small. All the qualitative conclusions made above are valid here, too. The contribution of the ETMD processes for the singlet dicationic state $Ne^{2+}(2p^{-2})[^1D]$ is negligibly small.

From this analysis we can conclude that the shapes of the ICD angular distributions in Fig. 5 are defined mainly by the contributions of the σ ICD electrons (two lobes of unequal intensities along the molecular axis), while the π and δ waves make the lobe in the direction of the left atom somewhat broader.

Now let us study the variation of the angular distributions as a function of R. In Fig. 7 we show the dependence of

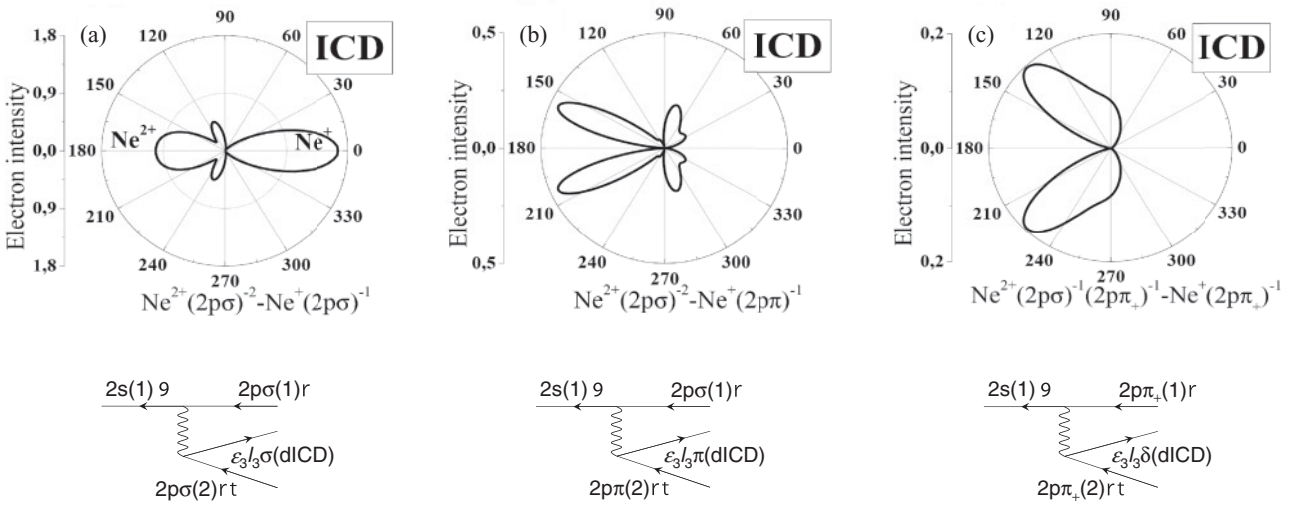

FIG. 6. Partial contributions to the ICD electron angular distributions corresponding to different states n' and n'' in Fig. 1(a); the corresponding Feynman diagram is shown near each figure. The calculations have been performed for $R = 5.16$ a.u., $k = 0.2$ with the frozen core wave functions. (a) The final state is $Ne^{2+}(2p\sigma)^{-2}$-$Ne^{+}(2p\sigma)^{-1}$, which corresponds to the σ ICD electron. (b) The final state is $Ne^{2+}(2p\sigma)^{-2}$-$Ne^{+}(2p\pi)^{-1}$, which corresponds to the π ICD electron. (c) The final state is $Ne^{2+}(2p\sigma)^{-1}(2p\pi_{+})^{-1}$-$Ne^{+}(2p\pi_{+})^{-1}$, which corresponds to the δ ICD electron.

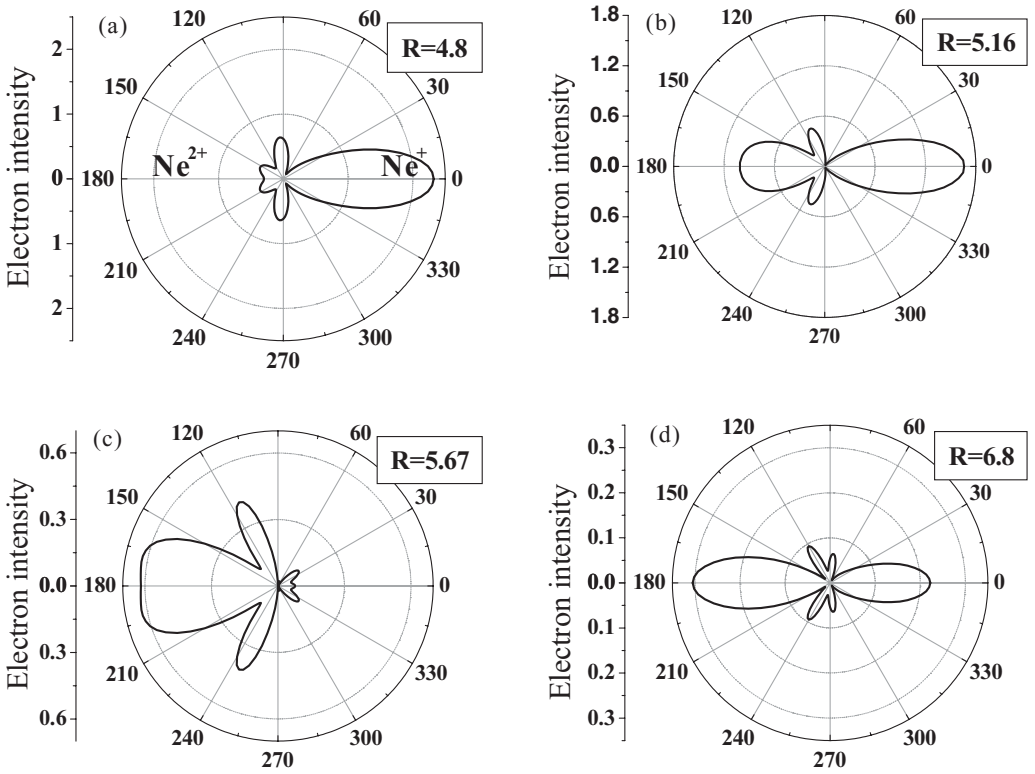

FIG. 7. The partial contribution to the ICD electron angular distribution shown in Fig. 6(a) for different internuclear distances R mentioned in the figures. The calculations have been performed with the frozen core wave functions. The doubly ionized neon atom is on the left side.

the angular distribution of the σ ICD electrons at different internuclear distances R with the corresponding ICD electron energies. The ICD electron is ejected from the right atom and is moving predominantly to the right side along the molecular axis. On the other hand, the electron can move also to the left side in the direction of the neighboring Ne atom, and after reflection from it the part of electron intensity returns back to the right and interferes with the original wave. The interference can be constructive and destructive depending on the phase shift difference between the two waves. The phase shift difference is estimated as $2kR$, where k is the electron momentum. At $R = 4.8$ a.u. and $k = 0.05$ we have $2kR = 0.48$. It means that there is a constructive interference, and the main lobe is directed to the right side [Fig. 7(a)]. At $R = 5.67$ a.u. and the ICD electron momentum $k = 0.343$, and we are getting $2kR = 3.88$, which means that to a good approximation the direct and reflected waves are in antiphase, and their interference essentially cancels the electron intensity to the right side. Practically all the electron intensity goes to the left side [Fig. 7(c)]. At two other internuclear distances, $R = 5.16, k = 0.2$ [Fig. 7(b)] and $R = 6.8, k = 0.477$ [Fig. 7(d)], the interference of two waves is less appreciable, and the left and the right lobes are comparable in magnitude. Comparison between these four angular distributions clearly shows that there is a substantial dependence on the internuclear distance, and the averaging over some interval of internuclear distances can smooth over this dependence. Therefore, knowing the dependence of the angular distributions on the internuclear distance one can select more appropriate regions for averaging over R (that is over the KER energies). In particular, the four regions around the internuclear distances shown in Fig. 7 would be a more successful choice.

Consider now the angular distribution of the electrons corresponding to the diagonal B in Fig. 4. These electrons are produced by the exchange ICD [Eq. (2) and Fig. 1(d)] and ETMD [Eq. (3a) and Fig. 1(e)] processes, leading to the triplet doubly charged ion $Ne^{2+}(2p^{-2})[^3P]$ in the final state. These processes create more energetic ions, which means that they take place at smaller internuclear distances than the decays into the singlet $Ne^{2+}(2p^{-2})[^1D]$ state. The experimental data correspond to the integration over the internuclear distances from $R = 3.9$ a.u. to $R = 4.8$ a.u.. Therefore, the first calculations have been performed for the internuclear distances $R = 4.3$ a.u. (KER = 13 eV) and for the electron energy 1.2 eV, which corresponds to the middle part of the diagonal B. The exchange ICD process is giving the contribution at least one order of magnitude larger than the ETMD; therefore, below we discuss only the eICD results. The main contribution is given again by the σ eICD electron which is ejected now from the left atom to the left and the right sides along the molecular axis. The wave ejected to the right after reflection from the right atom is moving back to the left side, acquiring the phase shift $2kR = 2.6$. To a good approximation this leads to a destructive interference and produces a small intensity of the eICD electrons to the left side, which is in agreement with the experimental data shown in Fig. 8. At another internuclear distance $R = 4.8 (k = 0.44)$ also shown in Fig. 8 the minimum at 180° disappears, leading to a better agreement with the experiment. Still the main intensity is

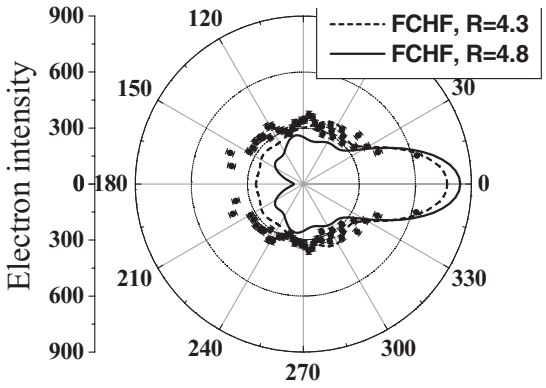

FIG. 8. The experimental and theoretical angular distributions of the ICD and ETMD electrons corresponding to the triplet final state $Ne^{2+}(2p^{-2})[^3P]$ [Eqs. (2) and (3a) (line B in Fig. 4)].

directed to the right side. There is a difference between two theoretical curves, and there is a reasonable agreement with the experiment if we take into account that there is the integration over the internuclear distances.

VI. SUMMARY

The detailed theoretical analysis of the experimental angular distributions of the ICD electrons from Ne dimers in the molecular frame has been performed. For the initial state we solve the self-consistent HF equations for the Ne_2^{2+} ion with two holes localized on the left atom as if it were a heteronuclear diatomic molecule. Two approximations have been used for calculations of the ICD or ETMD electron wave functions. In the frozen core approximation the basis of the doubly charged molecular ion wave functions was used to construct the potential for the final triply charged ion state in which the ICD electron is moving. In the relaxed core approximation the triply charged ion HF wave functions of the final state were calculated self-consistently and the ICD electron wave function was found in their field. The angular distributions of the electrons from the ICD processes into the singlet $Ne^{2+}(2p^{-2})[^1D]$ state found in these two approximations have been compared with the experimental data obtained from the electron-ion-ion coincident measurements using the COLTRIMS technique.

In the measurements the KER energies of two departing ions have been determined. Different KER energies correspond to different internuclear distances at which the ICD process takes place. In experiment for the singlet $Ne^{2+}(2p^{-2})[^1D]$ state the data have been presented for three regions of KER energies corresponding to integration over some region of the internuclear distances R, while the corresponding calculations have been performed for three fixed internuclear distances. The frozen core and relaxed core approximations give qualitatively similar results which are in a satisfactory agreement with the experiment. The main peculiarity of the angular distributions, the increase of the intensity in the direction of the Ne^+ ion with increasing KER energy (that is with decreasing of the internuclear distance R) is correctly reproduced by the theory. One can conclude that our method to describe the interatomic interaction in Ne_2 in spite of its relative simplicity is adequate. The difference between the frozen core and relaxed core calculations can be used as an estimation of contribution of the processes neglected in our approximation. The calculations at different internuclear distances demonstrated that the shapes of the angular distributions strongly depend on R. The measurement at a fixed KER energy gives the unique dynamical information on the decay process. Averaging over KER can smooth this dependence; therefore, for a better understanding of the dynamics of the ICD process it would be helpful to select narrower regions of KER energies in the experiment.

The other ICD decay into the triplet final ion state $Ne^{2+}(2p^{-2})[^3P]$ was also studied. Here the main contribution is given by the exchange ICD process shown in Fig. 1(d) while the ETMD contribution [Fig. 1(e)] is too small. The experimental data are obtained by integration over all KER energies where the process is observed. In general there is a reasonable agreement between theory and experiment. For the triplet state the dependence on R is less substantial.

ACKNOWLEDGMENTS

Fruitful discussions with Professor Lorenz Cederbaum and his group are greatly acknowledged. N.A.C. and S.K.S. acknowledge the financial support of Deutsche Forschungsgemeinschaft and the hospitality of the Goethe University in Frankfurt am Main. They also acknowledge the financial support of RFBR (Grant No 12-03-00825).

[1] M. Thompson, M. D. Baker, A. Christie, and J. F. Tyson, *Auger Electron Spectroscopy* (Wiley, New York, 1985).
[2] L. S. Cederbaum, J. Zobeley, and F. Tarantelli, Phys. Rev. Lett. **79**, 4778 (1997).
[3] R. Santra, J. Zobeley, L. S. Cederbaum, and N. Moiseyev, Phys. Rev. Lett. **85**, 4490 (2000).
[4] S. Marburger, O. Kugeler, U. Hergenhahn, and T. Möller, Phys. Rev. Lett. **90**, 203401 (2003).
[5] G. Öhrwall, M. Tchaplyguine, M. Lundwall, R. Feifel, H. Bergersen, T. Rander, A. Lindblad, J. Schulz, S. Peredkov, S. Barth, S. Marburger, U. Hergenhahn, S. Svensson, and O. Björneholm, Phys. Rev. Lett. **93**, 173401 (2004).
[6] S. Barth *et al.*, J. Chem. Phys. **122**, 241102 (2005).
[7] T. Jahnke, A. Czasch, M. S. Schöffler, S. Schössler, A. Knapp, M. Käsz, J. Titze, C. Wimmer, K. Kreidi, R. E. Grisenti, A. Staudte, O. Jagutzki, U. Hergenhahn, H. Schmidt-Böcking, and R. Dörner, Phys. Rev. Lett. **93**, 163401 (2004).
[8] T. Aoto, K. Ito, Y. Hikosaka, E. Shigemasa, F. Penent, and P. Lablanquie, Phys. Rev. Lett. **97**, 243401 (2006).
[9] T. Jahnke, A. Czash, M. Schöffler, M. Schössler, M. Käsz, J. Titze, K. Kreidi, R. E. Grisenti, A. Staudte, O. Jagutzki, L. Ph. H. Schmidt, S. K. Semenov, N. A. Cherepkov, H. Schmidt-Böcking, and R. Dörner, J. Phys. B **40**, 2597 (2007).
[10] L. S. Cederbaum and W. Domcke, J. Chem. Phys. **66**, 5084 (1977).

[11] D. Rolles, M. Braune, S. Cvejanojvi, O. Gessner, R. Hentges, S. Korica, B. Langer, T. Lischke, G. Prìmper, A. Reinköster, J. Viefhaus, B. Zimmermann, V. McKoy, and U. Becker, Nature (London) **437**, 711 (2005).
[12] M. S. Schöffler *et al*., Science **320**, 920 (2008).
[13] J.-I. Adachi, K. Hosaka, T. Teramoto, M. Yamazaki, N. Watanabe, M. Takahashi, and A. Yagishita, J. Phys. B **40**, F285 (2007).
[14] N. A. Cherepkov, S. K. Semenov, and R. Dörner, J. Phys.: Conf. Ser. **141**, 012001 (2008).
[15] R. Santra and L. S. Cederbaum, Phys. Rev. Lett. **90**, 153401 (2003).
[16] Y. Morishita, X.-J. Liu, N. Saito, T. Lischke, M. Kato, G. Prumper, M. Oura, H. Yamaoka, Y. Tamenori, I. H. Suzuki, and K. Ueda, Phys. Rev. Lett. **96**, 243402 (2006).
[17] K. Kreidi *et al*., J. Phys. B **41**, 101002 (2008).
[18] M. Yamazaki, J.-I. Adachi, Y. Kimura, A. Yagishita, M. Stener, P. Decleva, N. Kosugi, H. Iwayama, K. Nagaya, and M. Yao, Phys. Rev. Lett. **101**, 043004 (2008).
[19] N. A. Cherepkov *et al*., Phys. Rev. A **80**, 051404 (2009).
[20] S. K. Semenov *et al*., Phys. Rev. A **81**, 043426 (2010).
[21] N. A. Cherepkov *et al*., Phys. Rev. A **82**, 023420 (2010).
[22] S. D. Stoychev, A. I. Kuleff, F. Tarantelli, and L. S. Cederbaum, J. Chem. Phys. **129**, 074307 (2008).
[23] M. Ya. Amusia and N. A. Cherepkov, Case Stud. At. Phys. **5**, 47 (1975).
[24] I. Lindgren and J. Morrison, *Atomic Many-body Theory* (Springer, Berlin, 1986).
[25] K. Zähringer, H.-D. Meyer, and L. S. Cederbaum, Phys. Rev. A **45**, 318 (1992); **46**, 5643 (1992).
[26] R. Dörner, V. Mergel, O. Jagutzki, L. Spielberger, J. Ullrich, R. Moshammer, and H. Schmidt-Böcking, Phys. Rep. **330**, 95 (2000).
[27] K. Kreidi *et al*., Phys. Rev. A **78**, 043422 (2008).
[28] J. Ullrich, R. Moshammer, A. Dorn, R. Dörner, L. Ph. H. Schmidt, and H. Schmidt-Böcking, Rep. Prog. Phys. **66**, 1463 (2003).
[29] T. Jahnke, Th. Weber, T. Osipov, A. L. Landers, O. Jagutzki, L. Ph. H. Schmidt, C. L. Cocke, M. H. Prior, H. Schmidt-Böcking, and R. Dörner, J. Electron Spectrosc. Relat. Phenom. **141**, 229 (2004).
[30] O. Jagutzki, V. Mergel, K. Ullmann-Pfleger, L. Spielberger, U. Spillmann, R. Dörner, and H. Schmidt-Böcking, Nucl. Instrum. Methods A **477**, 244 (2002).